A transient ultraviolet outflow in the short-period X-ray binary UW CrB

S. Fijma,[1]★ N. Castro Segura,[2] N. Degenaar,[1] C. Knigge,[2] N. Higginbottom,[2] J. V. Hernández Santisteban,[3] T.J. Maccarone[4]

[1]*Anton Pannekoek Institute for Astronomy, University of Amsterdam, Science Park 904, 1098 XH, Amsterdam, the Netherlands*
[2]*Department of Physics & Astronomy. University of Southampton, Southampton SO17 1BJ, UK*
[3] *SUPA School of Physics & Astronomy, University of St Andrews, North Haugh, St Andrews KY16 9NS, Scotland, UK*
[4]*Department of Physics & Astronomy, Texas Tech University, Box 41051, Lubbock, TX, 79409-1051, USA*

Accepted XXX. Received YYY; in original form ZZZ

ABSTRACT

Accreting low mass X-ray binaries (LMXBs) are capable of launching powerful outflows such as accretion disc winds. In disc winds, vast amounts of material can be carried away, potentially greatly impacting the binary and its environment. Previous studies have uncovered signatures of disc winds in the X-ray, optical, near-infrared, and recently even the UV band, predominantly in LMXBs with large discs ($P_{\rm orb}\geq$20 hrs). Here, we present the discovery of transient UV outflow features in UW CrB, a high-inclination ($i\geq77^\circ$) neutron star LMXB with an orbital period of only $P_{\rm orb}\approx$111 min. We present P-Cygni profiles identified for Si IV 1400Å and tentatively for N V 1240Å in one 15 min exposure, which is the only exposure covering orbital phase $\phi\approx0.7-0.8$, with a velocity of $\approx$1500 km s^{-1}. We show that due to the presence of black body emission from the neutron star surface and/or boundary layer, a thermal disc wind can be driven despite the short $P_{\rm orb}$, but explore alternative scenarios as well. The discovery that thermal disc winds may occur in NS-LMXBs with $P_{\rm orb}$ as small as $\approx$111 min, and can potentially be transient on time scales as short as $\approx$15 min, warrants further observational and theoretical work.

Key words: accretion, accretion discs – stars: neutron – X-rays: binaries – stars: winds, outflows – ultraviolet: stars – binaries: eclipsing

1 INTRODUCTION

Accreting low mass X-ray binaries (LMXBs) are capable of producing powerful outflows. In addition to jets, LMXBs can launch winds from the accretion disc, which can have a great impact on both the binary and its local environment. As vast amounts of material can be carried away through disc winds (e.g. Lee et al. 2002; Ponti et al. 2012), the accretion process can be affected (e.g. Begelman et al. 1983; Muñoz-Darias et al. 2016; Tetarenko et al. 2018), and the long-term orbital evolution can be altered (e.g. Degenaar et al. 2014; Marino et al. 2019). Outflows can also heat and stir up the surrounding interstellar medium to stimulate star formation (e.g. Justham & Schawinski 2012). Therefore, studying disc winds is vital in gaining a deeper understanding of X-ray binary systems and how they evolve, accretion physics, binary evolution and the role of LMXB feedback.

Disc winds in LMXBs were initially detected using high-resolution X-ray spectroscopy through blue-shifted absorption features (e.g. Ueda et al. 1998; Miller et al. 2006; Neilsen & Lee 2009; Ponti et al. 2012). These features are proposed to result from 'hot' winds of highly ionised outflowing material. Disc winds have also been detected using optical and near-infrared observations, through e.g. blue-shifted absorption features and/or P-Cygni profiles. Whereas these 'cold' winds have occasionally been detected in longer wavelengths in the past (e.g. Bandyopadhyay et al. 1999), it was not until the last few years that these started to be detected more routinely (e.g. Muñoz-Darias et al. 2016; Sánchez-Sierras & Muñoz-Darias 2020).

Several key questions about disc winds remain, as it is currently not established exactly how these winds are launched, or how much mass is lost this way. Different mechanisms are suggested to launch disc winds in LMXBs, namely thermal (e.g. Woods et al. 1996; Higginbottom et al. 2018), radiative (e.g. Proga & Kallman 2002), and magnetic driving (e.g. Proga 2000; Chakravorty et al. 2016). However, determining the exact mechanism through observational studies has proven to be very challenging. Furthermore, the relationship between the detected hot (X-ray) and cold (optical/nIR) disc winds is not well understood yet, i.e. if these disc winds sample parts of the same outflow, or if these are resulting of two distinct outflows. Some recent studies have been performed using multi-wavelength campaigns (e.g. Castro Segura et al. 2022; Muñoz-Darias & Ponti 2022) supporting a multi-phase nature of disc winds.

A promising avenue of studying LMXB outflows is exploring features in the UV-band, as it bridges the gap between the optical/IR and X-ray band. Moreover, the UV-band contains strong line transitions of key elements like H, N, Si, O and C, and accretion disc spectra can peak in the UV-band as well (e.g. Hynes et al. 2000). Outflows have been discovered using high-resolution far-UV (FUV) spectroscopy in a few studies (e.g. Boroson et al. 2001; Ioannou et al. 2003; Bayless et al. 2010; Castro Segura et al. 2022), but this field is still relatively unexplored. One aspect that greatly complicates UV-studies is interstellar extinction, especially since most LMXBs are located in the Galactic plane where the extinction along our line of sight is high (see e.g. Bahramian & Degenaar 2022).

★ E-mail: s.c.fijma@uva.nl

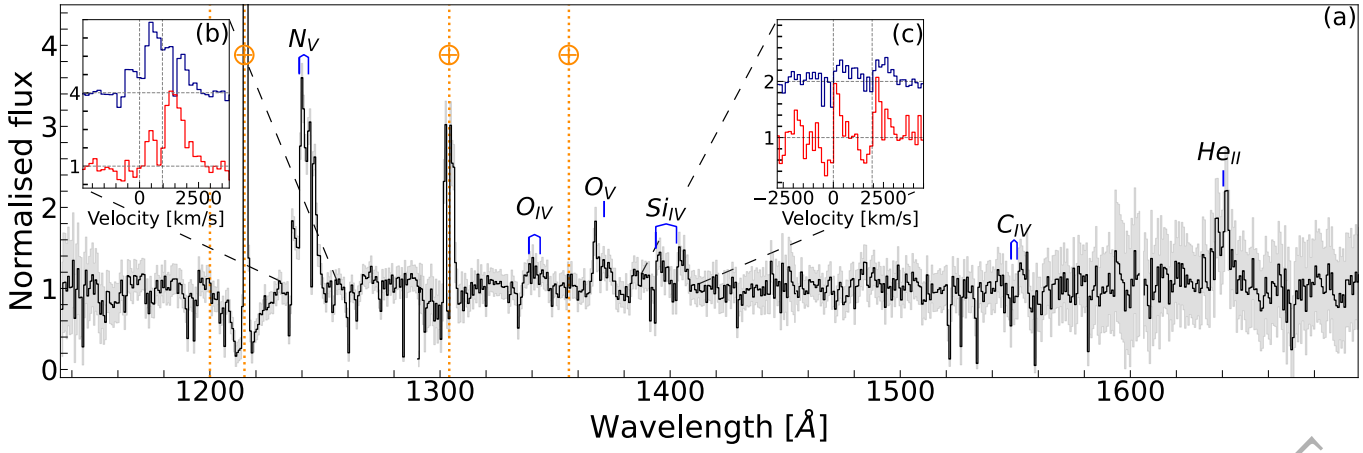

Figure 1. Panel (a): The normalised time-averaged FUV spectrum of UW CrB. The data of two gratings (G130M and G160M) are combined to cover ≈1150−1700Å, and are binned to 0.7Å resolution, the standard errors are shown in grey. Typical LMXB emission lines are labelled in blue. Terrestrial airglow emission features are marked in orange, and unlabelled narrow absorption features are interstellar. Insets (b) and (c) show the line profiles for N v and Si iv, respectively. The vertical grey dashed lines indicate the central line wavelengths of the doublets. The scaled normalised flux is plotted on the y-axis, and the velocity is plotted on the x-axis, where 0 km/s is centred with respect to the shorter wavelength of the doublet. The upper blue lines show the time-averaged spectra excluding data from Exposure 2. The bottom red line shows the spectra using only data from Exposure 2.

An intriguing target for a UV outflow study is the neutron star (NS) LMXB UW CrB. The interstellar extinction to UW CrB is relatively low, on the order of $N_{\rm H} \approx 4 \times 10^{20}$ cm^{-2} (HI4PI Collaboration et al. 2016) making it a suitable target to study in the UV. It was discovered by Morris et al. (1990) with *Einstein* at a flux level of $f_X \approx 1 \times 10^{-12}$ erg cm^{-2}s^{-1} (0.3-3.5 keV; Gioia et al. 1990). One explanation for the relatively low X-ray flux of UW CrB is that the central X-ray emitting region is obscured, as it is a high-inclination system with $77° \leq i \leq 81°$, based on the detection of eclipses both in the optical and X-ray band (Hakala et al. 2005; Hynes et al. 2004; Mason et al. 2008). It is suggested to have an elliptical and precessing accretion disc, based on a measured superhump-like modulation with a period of 5.5 days, as well as the variable eclipse depth. Moreover, the orbital period of the system is only $P_{\rm orb}$=110.98 minutes, indicating that UW CrB is a compact X-ray binary. This makes UW CrB an especially interesting target to search for disc winds, as disc winds have mostly been identified in LMXBs with an orbital period exceeding $\gtrsim$20 hours (see e.g. Díaz Trigo & Boirin 2016; Panizo-Espinar et al. 2022).

In this letter, we report on the discovery of transient outflow features in archival FUV data of UW CrB.

2 OBSERVATIONS, DATA ANALYSIS AND RESULTS

2.1 Data

The Hubble Space Telescope (*HST*) observed UW CrB on September 1, 2011 between 02:15 and 09:12 UT as part of the GTO/COS programme 12039 (PI Green). The data was acquired using the Cosmic Origins Spectrograph (COS; Green et al. 2012) in `TIME-TAG` mode using the primary science aperture. A total of ten exposures were obtained in five consecutive *HST* orbits, using two FUV (G130M and G160M) and one NUV (G230L) grating. The G130M grating samples wavelengths between ≈ 900−1450Å, the G160M grating between ≈ 1360−1775Å, and the G230L between ≈ 1650−3200Å. The total exposure time is 4.7 ks for the G130M, 5.6 ks for the G160M, and 2.9 ks for the G230L gratings. This yields a wavelength coverage of 1150−1800Å and an average spectral resolution of $R=\lambda/\Delta\lambda \approx 14000$ for the G130M and G160M gratings, and 1650−3200Å and $R \approx 2650$ for the G230L grating. We show the observation details in Table 1.

We used the *HST* `CalCOS` pipeline[1] to reduce the COS data. To exclude the emission from airglow lines, the geocoronal Lyman-α (1208 to 1225Å) and O I (1298 to 1312Å) line profiles were masked. We use the standard pipeline data products to obtain the one-dimensional spectra per exposure. We resampled the one-dimensional spectra on to a common wavelength grid using adapted code from the `SpectRes` package (Carnall 2017). To achieve time-resolved spectroscopy, we use the `costools splittag` package to split the TIME-TAG data into sub-exposures. Light curves are extracted from the TIME-TAG events lists as described in Castro Segura et al. (2022) using adapted code from the `lightcurve`[2] package.

2.2 Spectral analysis

In Figure 1 we show the combined FUV spectrum. We have not corrected the spectrum for interstellar extinction, since the estimate for the reddening along the line of sight is low, and is not expected to significantly affect the spectrum. We also do not detect the 2175Å dust feature used by other studies to perform dereddening (e.g., Froning et al. 2011), suggesting that $E(B-V) \lesssim 0.05$ (e.g. Verbunt 1987).

The FUV spectrum features strong emission lines, such as O iv 1343Å, O v 1371Å, the Si iv 1400Å doublet and He ii 1640Å. Most notably, it shows a strong N v 1240Å (doublet) line, while the C iv 1549Å doublet is barely identified. As these lines are both resonance lines of lithium-like ions, and as they are produced under similar physical conditions, this suggests an under-abundance of carbon in the surface layers of the donor star (see e.g. Haswell et al. 2002). This material is therefore likely to have undergone substantial CNO processing, so the donor star of this system could be an evolved main-sequence star (see also Froning et al. 2011, 2014, Castro Segura et al. in prep, on other LMXBs).

[1] https://github.com/spacetelescope/calcos
[2] https://github.com/justincely/lightcurve

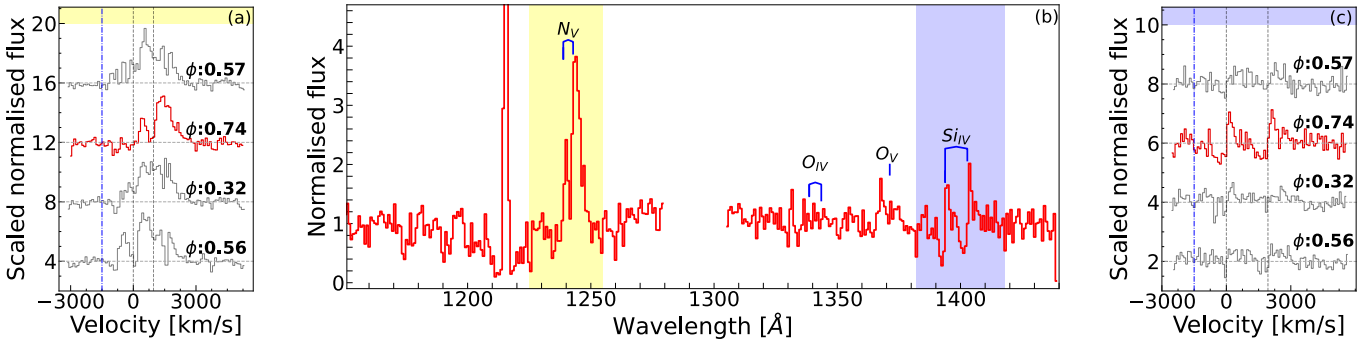

Figure 2. The outflow features detected in UW CrB. Panel (a) and (c) show the N v and Si iv line profiles in velocity space for all the available exposures, with the average orbital phase (ϕ) per exposure indicated, and Exposure 2 shown in red. The vertical grey dashed lines indicate the central line wavelengths of the doublets, and the blue dash-dotted lines indicate where the velocity is −1500 km/s with respect to the shorter wavelength of the doublet. Panel (b) shows the blue portion of the normalised FUV spectrum of the exposure of UW CrB showing the transient far-UV outflow features (Exposure 2) detected in Si iv 1400Å and N v 1240Å. The spectrum is binned to 0.8Å resolution.

HST exp.	Time (UT)	Grating	Central wlen (Å)	T_{exp} (s)	Orbital phase (ϕ)
Exp 1	02:23:49	G130M	1291	1044.192	0.57 ± 0.08
Exp 2	02:43:01	G130M	1300	884.192	0.74 ± 0.07
Exp 3	03:47:03	G130M	1309	1400.192	0.32 ± 0.11
Exp 4	04:13:17	G130M	1318	1393.184	0.56 ± 0.11
Exp 5	05:22:54	G160M	1577	1400.160	0.18 ± 0.11
Exp 6	05:49:07	G160M	1600	1391.168	0.42 ± 0.10
Exp 7	06:58:41	G160M	1611	1400.192	0.05 ± 0.11
Exp 8	07:24:55	G160M	1623	1393.120	0.28 ± 0.11
Exp 9	08:33:58	G230L	2950	1393.208	0.91 ± 0.11
Exp 10	09:00:13	G230L	3360	1464.224	0.14 ± 0.11

Table 1. Observation summary. The time in UT is on 2011-09-01 for mid-observation. The average orbital phase and range is indicated for each exposure. The uncertainty for the orbital phase for all exposures is around $\pm 0.01\,\phi$.

In the combined spectrum and in the individual spectra per exposure, we see little to no emission for the C iv 1550Å line. There appears to be a hint of a C iv emission line in the sub-exposure covering around $\phi \approx 0.05-0.15$, but it is not statistically significant. We also find that the He ii 1640Å line appears single-peaked in the combined spectrum and in the individual spectra per exposure. However, only in the sub-exposure covering the eclipse $\phi \approx 0.95-0.05$, the line appears double peaked. As this appears when the companion star eclipses the compact object and the disc, this could potentially be resulting of the irradiated side of the donor star also emitting a single-peaked He ii during other parts of the orbital phase, which is super-imposed onto the double peaked He ii disc line. However, we currently have insufficient data to confirm this, and we are also unsure how this relates to the detection of C iv in the sub-exposure after this. Both the characterisation of these lines, as well as CNO processing of the donor star, will be explored in a separate work on UW CrB. Finally, no significant lines (including e.g. Mg II 2800Å) are detected in the NUV spectrum.

When studying the spectra from the individual exposures, we find that the Si iv 1400Å line profile shows clear P-Cygni profiles in one exposure. Moreover, the N v 1240Å line shows tentative evidence of associated blue-shifted absorption in this same exposure. We show the spectrum of this exposure, as well as the Si iv and N v line profiles in Figure 2. As these lines are created at a similar temperature of around $T \approx 10^4$ K, this establishes the presence of warm outflowing material in UW CrB. However, these P-Cygni features are only detected in one of the ten total exposures (Exposure 2, specifically).

2.3 Outflow features

In Figure 2, we show that the edge of the transient blue-shifted absorption features for Si iv and N v in Exposure 2 extend to around $v \approx -1500$ km/s from the central line-wavelengths, giving us the approximate terminal velocity of the outflowing material. We also find that the blue-shifted absorption troughs for both Si iv and N v reach a similar level below the continuum, around 50 percent.

In Figure 2, we also show the line profiles of Si iv and N v for the other available exposures. The P-Cygni profiles for Si iv are only clearly detected in Exposure 2. In other exposures, there appear to be narrow absorption features with the width of the spectral resolution. However, we are not sure if these can be attributed to an outflow. Since they are at the rest position of Si iv, these could also potentially be formed by interstellar absorption. Therefore, we can only confidently identify outflow features in Exposure 2.

The exposures taken with the G160M grating cover the red portion of the FUV spectrum, and include lines such as He ii and C iv. As mentioned in Section 2.2, there is little to no emission for the C iv line, but the He ii line is quite strong. We do not identify significant blue-shifted absorption and/or P-Cygni features for the C iv or He ii lines.

Detecting blue-shifted absorption associated with UV resonance lines, such as Si iv and N v, suggests that the outflowing material has a significant optical depth for these transitions. Based on the required minimum column densities, lower limits can placed on the mass-loss rate, as determined by Castro Segura et al. (2022). In this work, they rewrite the equation for the optical depth as defined in Eq. 9 of Drew (1987), to a characteristic optical depth for C iv 1549Å of:

$$\tau \simeq 33.6 \left(\frac{f_{osc}}{0.2847}\right)\left(\frac{\lambda}{1549}\right)\left(\frac{A}{3\times10^{-4}}\right)\left(\frac{f_{ion}}{1}\right)\left(\frac{\dot{M}_{wind}}{10^{-10}M_\odot yr^{-1}}\right)\left(\frac{r}{10^{10}cm}\right)^{-1}\left(\frac{v(r)}{1500kms^{-1}}\right)^{-2} \quad (1)$$

Where f_{osc} and λ are the oscillator strength and the wavelength of the line, A the abundance of the relevant element relative to hydrogen, f_{ion} the fraction of those atoms at the correct ionisation level, $\dot{M}_{wind}$ the mass-loss rate of the outflow, and r the radius where velocity

$v(r)$ is reached. The reference values for the velocity $v(r)$ is set on the estimated velocity of the UV outflow, and r on the radius where a thermally driven wind could be launched (see Section 3). $f_{\rm ion}$ is set to 1 to ensure that the estimate for $\dot{M}_{\rm wind}$ is a lower limit. For Si IV 1400Å and N V 1240Å, the reference value for A is based on solar abundances obtained from Lodders et al. (2009), which are 3.41×10^{-5} and 7.24×10^{-5} for these lines, respectively. The reference value for $f_{\rm osc}$ is adopted from Morton (2003), which are 0.767 and 0.234 for the lines, respectively. With the assumption that $\tau\gtrapprox1$ based on the depth of the lines, the estimated lower limits on the mass-loss rates are $\dot{M}_{\rm wind}\gtrapprox 1.11\times10^{-11}\,{\rm M}_\odot{\rm yr}^{-1}$ for Si IV, and $\dot{M}_{\rm wind}\gtrapprox 1.89\times10^{-11}\,{\rm M}_\odot{\rm yr}^{-1}$ for N V. This calculation does assume a symmetric persistent outflow, see Section 2.4 and 3 for discussion on the nature of the detected outflow.

2.4 Light curve

To study the time-dependent properties of the outflow, we study the extracted FUV light curve. Mason et al. (2012) calculated the eclipse ephemeris of UW CrB using a total of 56 eclipses spanning 20 years, allowing us to determine the orbital phase of the *HST* observations.

We show the light curve obtained from the FUV *HST* COS data in Figure 3, with the phase-folded light curve shown in the upper panel (a), and the full light curve shown in lower panel (b). From the phase-folded light curve we find that the lowest UV flux is found at $\phi\approx0$, which is expected to be the center of the eclipse. The lowest flux is not exactly at ϕ=0, which could be due to the orbital phase of mid-eclipse wandering by up to $\Delta\phi\pm0.08$ (Mason et al. 2012) and the uncertainty on the orbital phase being around $\pm0.011\phi$.

We find that the exposure where we detect the outflow features (Exposure 2), is the only exposure covering the orbital phase range $\phi\approx0.7-0.8$. Therefore, it could be that the presence of outflows (or the strength of their features) is dependent on the orbital phase. Other parts of the orbital phase range are covered by one or more exposures, but no outflow features are confidently identified here. Alternatively, it could be a transient outflow. Optical P-Cygni profiles have been observed during flaring activity of some BH-LMXBs (e.g. Muñoz-Darias et al. 2016; Muñoz-Darias & Ponti 2022). However, we do not identify any flaring components in the UV light curve.

Lastly, the outflow features could also appear transient due to line-of-sight effects. Based on complex variations in the optical and X-ray light curves, Mason et al. (2008) and Hakala et al. (2009) suggest that UW CrB has a precessing elliptical accretion disc. Mason et al. (2012) also discuss that variations in the optical light curve could be caused by an out-of-plane structure such as a non-axisymmetric flared or warped accretion disc, or a non-axisymmetric disc wind (as observed for X1822-371; see e.g. Bayless et al. 2010). This could be causing the large-amplitude variations in the UV light curve. The outflowing material could therefore potentially be obscured from the line-of-sight, resulting in the transient UV outflow features.

2.5 Time-resolved spectroscopy

To explore the time-dependent properties of the outflow in more detail, we split each original exposure in two, to have enough signal in each sub-exposure. In Figure 4 we show sub-exposures of the Si IV and N V lines. We find that the P-Cygni profiles found for Si IV and N V do not appear to change significantly in time during Exposure 2, as shown for the two sub-exposures indicated in red. In all other sub-exposures, we find no clear evidence of P-Cygni profiles for any of the lines in the spectrum. There appear to be hints of associated blue-shifted absorption features for Si IV in the sub-exposures preceeding Exposure 2. However, we do not see this for the N V line.

The line profile of N V appears to change during the (sub-)exposures. The line appears double peaked during some (sub-)exposures, and single peaked during others. Moreover, the line centres of the two identified peaks for N V also appear to shift, between around ≈−500 to 500 km/s. However, it is not clear if these are the two peaks of the doublet, or if the narrow left-most peak is a separate feature. Furthermore, it is unclear if the shift in the line-centres is related to a doppler-shift, or if this is related to other changes in the line-profile, especially since it appears differently for sub-exposures covering similar parts of the orbital phase. Therefore, it appears difficult to identify an outflow based on this line alone.

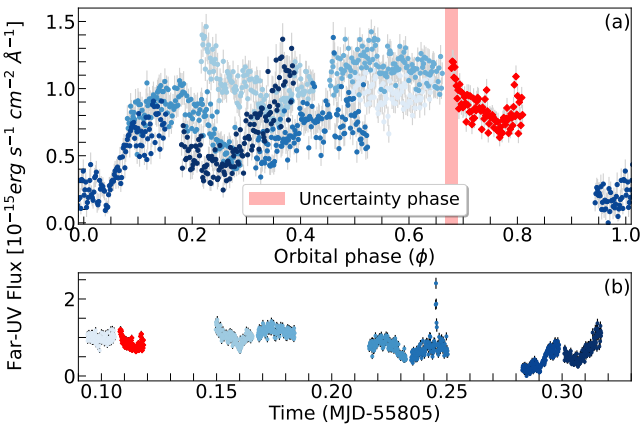

Figure 3. The light curve for all the FUV *HST* COS exposures. The exposure where the outflow features are detected (Exposure 2) is shown in red, and other exposures are indicated with blue sequential colours from light to dark to show the evolution in time. A type-I burst is identified around MJD 55805.23, but is cropped from panel (a) for clarification. Upper panel (a) shows the phase-folded light curve, where orbital phase ϕ=0 indicates the mid-point of the eclipse. The uncertainty on the orbital phase is indicated with a red bar. Lower panel (b) shows the light curve plotted with time on the x-axis in days.

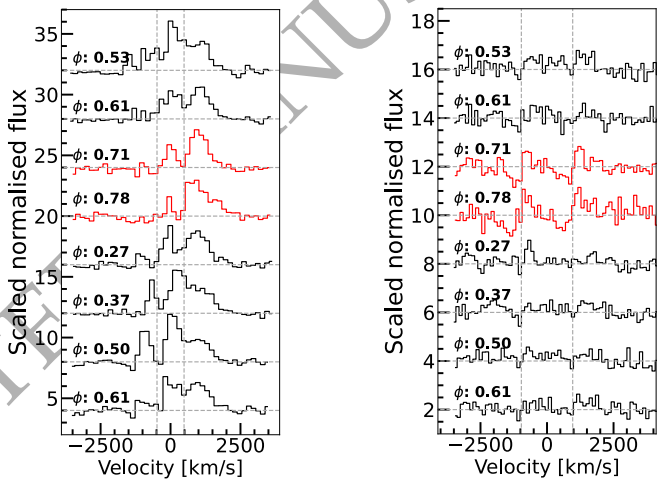

Figure 4. The N V 1240Å (right panel) and Si IV 1400Å (left panel) lines in the time-resolved spectra of sub-exposures of UW CrB. The average orbital phase of the sub-exposures are indicated on the upper-left, within a range of around $\Delta\phi\pm0.04$. The sub-exposures of Exposure 2 are indicated in red. The other sub-exposures are indicated in black.

However, because of the clear P-Cygni profiles found for Si IV in Exposure 2, we tentatively associate the blue-shifted absorption for N V in the same exposure with the detected outflow. The evolution of the N V line profile should be further explored in future research.

3 DISCUSSION

Based on our detection of the transient UV outflow features for UW CrB, we explored if outflow features are detected in archival studies using other wavebands. Morris et al. (1990) present optical spectra of UW CrB, and note that the He I lines are systematically blue-shifted relative to the emission lines, potentially indicating a cool outflow. Hakala et al. (2005) present 0.2-10 keV X-ray spectra. NS-LMXBs typically show broad Fe-K emission lines, interpreted as reflection from the inner disc (e.g. Cackett et al. 2008). However, the emission line in the X-ray spectrum of UW CrB appears narrow. While not conclusive, this may indicate that it results from scattering in a wind instead of disc reflection (e.g. Titarchuk et al. 2009).

We can consider what types of outflows would be possible in this system, starting with the scenario of disc winds. The estimated velocity of 1500 km s^{-1} is consistent with the outflow speeds detected for (thermally-driven) disc winds (see overviews in e.g. Díaz Trigo & Boirin 2016; Panizo-Espinar et al. 2022, for other wavebands). Thermally driven winds can be launched from 10 percent of the Compton radius (Begelman et al. 1983), which is the radius at which the local isothermal sound speed (at the Compton temperature, $T_{\rm IC}$) is equal to the escape velocity in the disc. It is defined as $R_{\rm IC}=\frac{GM\mu m_{\rm H}}{k_{\rm B}T_{\rm IC}}$, where M is the mass of the central object and μ is the mean molecular mass. We assume M=1.4M$_\odot$ for a neutron star, and that μ=0.6 and $T_{\rm IC}$=1.4 $\times$ 10^7 K as in Higginbottom et al. (2017), resulting in $R_{\rm IC}\approx9\times10^{10}$ cm for UW CrB. To estimate the size of the disc, we can use two methods. We can calculate the circularisation radius, which is the radius within which the accretion disc is formed from the accretion flow, or the 3:1 resonance radius, which is the radius at which the disc is expected to be truncated for systems with low eccentricity. For both calculations, we use the mass-ratio $q\approx0.15$, the mass $M_1\approx1.4$ M$_\odot$ for the compact object, and the mass $M_2\approx0.2$ M$_\odot$ for the companion star, as proposed by Mason et al. (2008). We find both the circularisation and 3:1 resonance radius are around $R\approx4\times10^{10}$ cm, thus the disc likely exceeds $0.1R_{\rm IC}$ needed to launch a thermal wind.

To explore this a bit further, we have modelled the expected thermal stability curves for UW CrB, following the procedure of Higginbottom et al. (2017). Briefly, we use the radiative transfer and ionization code PYTHON (Long & Knigge 2002; Higginbottom et al. 2018, 2019, 2020) to determine the physical conditions in an irradiated, optically thin parcel of gas. The conditions in such a parcel are controlled by two factors: (i) the spectral energy distribution of the radiation field, and (ii) the strength of the irradiation. As the central X-ray source of UW CrB is likely obscured, we do not have access to the intrinsic spectral energy distribution (SED) of the system. We therefore use the simple, but flexible analytical model $F_\nu=\nu^{-0.2}\exp(-h\nu/k_{\rm B}T_{\rm X})$ to describe the SED. This form was proposed for the NS-LMXBs 4U 0614+091 in Migliari et al. (2010), which has $P_{\rm orb}$ and $L_{\rm X}$ comparable to UW CrB.

Out of the few NS-LMXBs with reported SEDs, the SED of 4U 0614+091 seems most representative for UW CrB, despite the factor $\approx$2 difference in $P_{\rm orb}$. It is important to note that this analysis is sensitive to the details of the SED, and is mainly used as a proof-of-principle study to probe thermal wind launching in compact LMXBs.

We then consider two different possibilities: (i) $T_{\rm X}\approx4\times10^6$ K, representating a disc black body SED, and (ii) $T_{\rm X}\approx1.3\times10^7$ K, representating a central black body SED. The strength of the irradiation is controlled by the ionization parameter $\xi=L_{\rm X}/nR^2$, where $L_{\rm X}$ is the source luminosity, n is the gas density and R is the distance of the gas parcel from the source. As shown in Fig. 5, the stability curve is then a plot of the equilibrium temperature, $T_{\rm eq}$, against $\xi/T_{\rm eq}$ (which traces the ratio of radiation to gas pressure). Moving from left to right on this plot corresponds to moving vertically upwards in the irradiated atmosphere. The gas is thermally stable (unstable) if the slope of $T_{\rm eq}(\xi/T_{\rm eq})$ is positive (negative). In order to launch a powerful irradiation-driven outflow, the material in the disc atmosphere needs to experience rapid runaway heating, i.e. it needs to become thermally unstable at some critical height in the atmosphere. Fig. 5 shows that this condition is not met for the cooler 'disc' SED, which is thermally stable everywhere. However, the hotter 'central black body' SED, representing emission from the NS surface and/or boundary layer, becomes thermally unstable at a critical ionization parameter $\xi_{\rm cool,max}=44.2$. In this case, material in the atmosphere would experience explosive heating, and a strong thermally-driven wind is likely to be launched.

We also explored the possibility of other wind driving mechanisms, i.e. radiative and magnetic driving. Radiation pressure due to electron scattering can assist thermal expansion to drive a disc wind if the luminosity is within around a factor of $\approx$2 of the Eddington limit (see e.g. Proga & Kallman 2002). Based on the known $P_{\rm orb}$ and measured optical brightness, we can use the relation of van Paradijs & McClintock (1994) to estimate the intrinsic $L_{\rm X}$, which suggests it is on the order of $\approx0.1L_{\rm EDD}$. Such an accretion luminosity would be consistent with the amplitude, recurrence rate and duration of the type-I bursts reported by e.g. Hakala et al. (2005). Therefore, we conclude that the outflow is unlikely to be caused by a radiatively driven wind in UW CrB. On the other hand, magnetic field lines threading the disc can launch a wind anywhere in the disc (see e.g. Chakravorty et al. 2016). Based on our data, we were unable to confirm or exclude a magnetically driven disc wind.

Finally, we briefly consider a few other possible scenarios for the outflow in UW CrB. Firstly, the P-Cygni profiles could alternatively have formed in a wind of matter evaporating from the atmosphere of the companion star. Some NS-LMXBs such as EXO 0748-676 are proposed to ablate material from the companion star, through a pulsar wind or X-ray heating (see e.g. Ratti et al. 2012; Knight et al. 2022). Secondly, we note that the estimated velocity of the UV outflow of $\approx$1500 km s^{-1} is around the Keplerian velocity of the outer disc in UW CrB (see e.g. Frank et al. 1987). So potentially, the detected outflow could result from the accretion stream and/or the hot spot where the accretion stream impacts the disc. This hot spot is expected to be visible at orbital phase $\phi\approx0.6$–0.8 (Frank et al. 1987; Ioannou et al. 2002) which matches the orbital phase where the UV outflow is detected. However, little is known about such outflows. Follow-up observations are needed to study possible phase-dependence of the outflow, and to confirm outflow features in optical and X-ray.

ACKNOWLEDGEMENTS

We thank M. Middleton, J. Matthews, M. Diaz Trigo and K. Long for useful discussions, and M. Stoop for helpful comments. SF and ND acknowledge the hospitality of the University of Southampton, where part of this research was carried out. This research is based on observations made with the NASA/ESA Hubble Space Telescope obtained from the Space Telescope Science Institute, which is operated by the Association of Universities for Research in Astronomy, Inc., under NASA contract NAS 5–26555. These observations are associated with program(s) 12039.

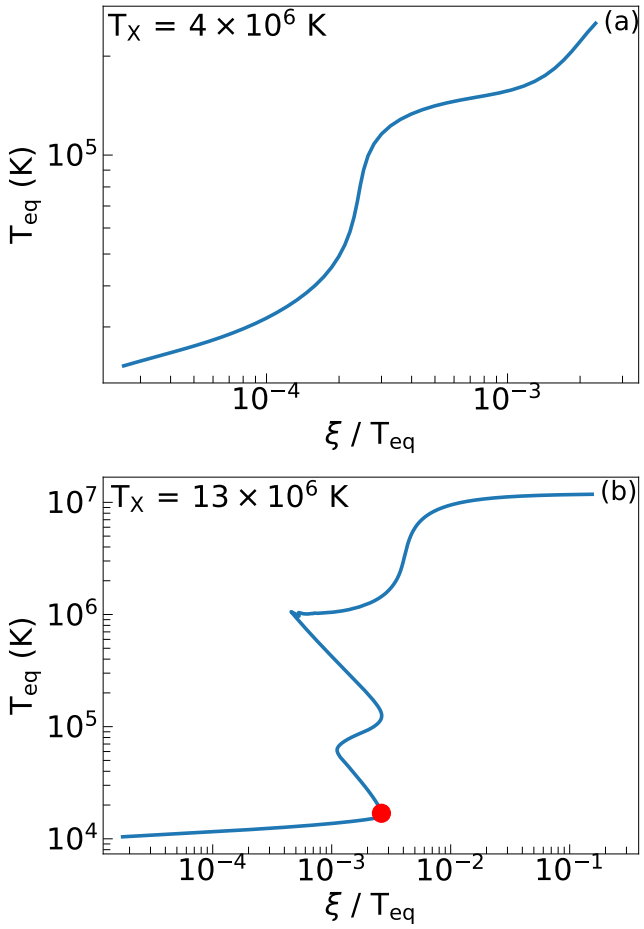

Figure 5. Thermal stability curves modelled for UW CrB, using a disc black body (Panel a) and a central black body (Panel b). The red dot in Panel b indicates the critical ionization parameter; $\xi_{\rm cool,max} = 44.2$.

DATA AVAILABILITY

The data underlying this article will be available in Zenodo at DOI: 10.5281/zenodo.7883747 upon publication. This astrophysical data set was retrieved from archival UV data from sources in the public domain: `https://mast.stsci.edu/search/ui/#/hst`.

REFERENCES

Bahramian A., Degenaar N., 2022, arXiv e-prints, p. arXiv:2206.10053
Bandyopadhyay R. M., Shahbaz T., Charles P. A., Naylor T., 1999, MNRAS, 306, 417
Bayless A. J., Robinson E. L., Hynes R. I., Ashcraft T. A., Cornell M. E., 2010, ApJ, 709, 251
Begelman M. C., McKee C. F., Shields G. A., 1983, ApJ, 271, 70
Boroson B., Kallman T., Vrtilek S. D., 2001, ApJ, 562, 925
Cackett E. M., et al., 2008, ApJ, 674, 415
Carnall A. C., 2017, arXiv e-prints, p. arXiv:1705.05165
Castro Segura N., et al., 2022, Nature, 603, 52
Chakravorty S., et al., 2016, A&A, 589, A119
Degenaar N., et al., 2014, ApJ, 784, 122
Díaz Trigo M., Boirin L., 2016, Astronomische Nachrichten, 337, 368
Drew J. E., 1987, MNRAS, 224, 595
Frank J., King A. R., Lasota J. P., 1987, A&A, 178, 137
Froning C. S., et al., 2011, ApJ, 743, 26
Froning C. S., Maccarone T. J., France K., Winter L., Robinson E. L., Hynes R. I., Lewis F., 2014, ApJ, 780, 48
Gioia I. M., Henry J. P., Maccacaro T., Morris S. L., Stocke J. T., Wolter A., 1990, ApJ, 356, L35
Green J. C., et al., 2012, ApJ, 744, 60
HI4PI Collaboration et al., 2016, A&A, 594, A116
Hakala P., Ramsay G., Muhli P., Charles P., Hannikainen D., Mukai K., Vilhu O., 2005, MNRAS, 356, 1133
Hakala P., Hjalmarsdotter L., Hannikainen D. C., Muhli P., 2009, MNRAS, 394, 892
Haswell C. A., Hynes R. I., King A. R., Schenker K., 2002, MNRAS, 332, 928
Higginbottom N., Proga D., Knigge C., Long K. S., 2017, ApJ, 836, 42
Higginbottom N., Knigge C., Long K. S., Matthews J. H., Sim S. A., Hewitt H. A., 2018, MNRAS, 479, 3651
Higginbottom N., Knigge C., Long K. S., Matthews J. H., Parkinson E. J., 2019, MNRAS, 484, 4635
Higginbottom N., Knigge C., Sim S. A., Long K. S., Matthews J. H., Hewitt H. A., Parkinson E. J., Mangham S. W., 2020, MNRAS, 492, 5271
Hynes R. I., Mauche C. W., Haswell C. A., Shrader C. R., Cui W., Chaty S., 2000, ApJ, 539, L37
Hynes R. I., Robinson E. L., Jeffery E., 2004, ApJ, 608, L101
Ioannou Z., Naylor T., Smale A. P., Charles P. A., Mukai K., 2002, A&A, 382, 130
Ioannou Z., van Zyl L., Naylor T., Charles P. A., Margon B., Koch-Miramond L., Ilovaisky S., 2003, A&A, 399, 211
Justham S., Schawinski K., 2012, MNRAS, 423, 1641
Knight A. H., Ingram A., Middleton M., Drake J., 2022, MNRAS, 510, 4736
Lee J. C., Reynolds C. S., Remillard R., Schulz N. S., Blackman E. G., Fabian A. C., 2002, ApJ, 567, 1102
Lodders K., Palme H., Gail H. P., 2009, Landolt Börnstein, 4B, 712
Long K. S., Knigge C., 2002, ApJ, 579, 725
Marino A., et al., 2019, A&A, 627, A125
Mason P. A., Robinson E. L., Gray C. L., Hynes R. I., 2008, ApJ, 685, 428
Mason P. A., Robinson E. L., Bayless A. J., Hakala P. J., 2012, AJ, 144, 108
Migliari S., et al., 2010, ApJ, 710, 117
Miller J. M., Raymond J., Fabian A., Steeghs D., Homan J., Reynolds C., van der Klis M., Wijnands R., 2006, Nature, 441, 953
Morris S. L., Liebert J., Stocke J. T., Gioia I. M., Schild R. E., Wolter A., 1990, ApJ, 365, 686
Morton D. C., 2003, ApJS, 149, 205
Muñoz-Darias T., Ponti G., 2022, A&A, 664, A104
Muñoz-Darias T., et al., 2016, Nature, 534, 75
Neilsen J., Lee J. C., 2009, Nature, 458, 481
Panizo-Espinar G., et al., 2022, A&A, 664, A100
Ponti G., Fender R. P., Begelman M. C., Dunn R. J. H., Neilsen J., Coriat M., 2012, MNRAS, 422, L11
Proga D., 2000, ApJ, 538, 684
Proga D., Kallman T. R., 2002, ApJ, 565, 455
Ratti E. M., Steeghs D. T. H., Jonker P. G., Torres M. A. P., Bassa C. G., Verbunt F., 2012, MNRAS, 420, 75
Sánchez-Sierras J., Muñoz-Darias T., 2020, A&A, 640, L3
Tetarenko B. E., Lasota J. P., Heinke C. O., Dubus G., Sivakoff G. R., 2018, Nature, 554, 69
Titarchuk L., Laurent P., Shaposhnikov N., 2009, ApJ, 700, 1831
Ueda Y., Inoue H., Tanaka Y., Ebisawa K., Nagase F., Kotani T., Gehrels N., 1998, ApJ, 492, 782
Verbunt F., 1987, A&AS, 71, 339
Woods D. T., Klein R. I., Castor J. I., McKee C. F., Bell J. B., 1996, ApJ, 461, 767
van Paradijs J., McClintock J. E., 1994, A&A, 290, 133